Absolute instability in backward wave four-wave mixing: spatial effects

Pierre Mathey,[1,*] Hans-Rudolf Jauslin,[1] Gregory Gadret,[1] Gary Cook,[2,3] Dean R. Evans,[2] and Serguey Odoulov[4]

[1]*Laboratoire Interdisciplinaire Carnot de Bourgogne, UMR 5209 CNRS-Université de Bourgogne, 9 Avenue Alain Savary, BP 47870, 21078 Dijon Cedex, France*
[2]*Air Force Research Laboratory, Materials and Manufacturing Directorate, Wright-Patterson Air Force Base, Ohio 45433, USA*
[3]*Azimuth Corporation, 4134 Linden Avenue, Suite 300, Dayton, Ohio, USA*
[4]*Institute of Physics, National Academy of Sciences, 03 650 Kyiv, Ukraine*
**Corresponding author: pmathey@u-bourgogne.fr*

Received April 16, 2010; accepted May 24, 2010;
posted May 28, 2010 (Doc. ID 127118); published June 24, 2010

The spatial distribution of new beams generated above the threshold of absolute instability of two counterpropagating incoherent light waves is studied and compared with the results of calculation. © 2010 Optical Society of America

OCIS codes: 190.5330, 190.4380, 160.2260.

1. INTRODUCTION

The high sensitivity of the oscillation dynamics of a semilinear coherent oscillator to possible misalignment of two counterpropagating pump waves has been reported recently [1,2]. Considerable changes in oscillation spectra and oscillation intensity were detected for misalignment angles on the order of one milliradian and even smaller. These misalignment angles are comparable to the divergence of the laser pump waves. The discovery of such a hypersensitivity became possible in part because of use of $KNbO_3$:Fe,Ag [3] and $BaTiO_3$:Co crystals with the enhanced nonlinear response at high spatial frequencies thus allowing for efficient recording of the reflection grating. The origin of these effects nests in the improvement of the phase conjugate reflectivity of the backward wave four-wave-mixing conjugator with a deliberately introduced phase mismatch [4,5].

The computer simulations and the linear stability analysis performed in [6] revealed also a similar sensitivity for absolute instability in backward wave four-wave mixing, i.e., for the appearance, at a certain critical coupling strength, of a conjugate beam with no signal beam at the input [7] (often referred to as a mirrorless oscillation). The calculations of paper [6] confirmed the lower threshold of mirrorless oscillation in the case of pump wave misalignment and predicted that the frequency detuning of the mirrorless oscillation tends to zero in the vicinity (but not exactly) of the threshold minima.

The subject of this paper is the study of the spatial orientation of the new beams generated above the critical point of the instability. It is shown that (*i*) the angular position of the oscillation beam is dictated by the requirement of the smallest threshold, i.e., the oscillation waves and the pump waves are misaligned in such a way that the total wavevector mismatch $\mathbf{\Delta}$ is constant and corresponds to the smallest possible threshold beam coupling, (*ii*) most often the oscillation wave propagating in each direction is split into two components, one with a positive and the other with a negative wave-vector mismatch $\mathbf{\Delta}$, (*iii*) the orientation of the oscillation waves depends on the plane of the pump wave misalignment while (*iv*) for perfectly aligned pump waves the orientation of $\mathbf{\Delta}$ is not defined and the oscillation develops along the conical surface centered on propagation direction of the pump waves. From the practical point of view it is important that a relatively small tilt of one of the two pump waves leads to a great change of the oscillation wave orientation.

2. EXPERIMENT

The experiments are performed with two $KNbO_3$:Fe,Ag samples, referred to as crystals A and B in this paper. Both crystals were modified post-growth using an indiffusion technique during the poling process. The result of the optical and holographic properties of these crystals depends on both the poling recipe and the type of electrode. In this particular case, Ag electrodes were used for poling and indiffusion [8]. Crystal A was inhomogeneously modified through indiffusion in a manner such that there exist two distinct regions, one which has a fast photorefractive response (a region with an obvious indiffusion) and the other which is significantly slower (a region which appears to have had no indiffusion); it has dimensions $4 \times 8 \times 7$ mm^3 along the x, y, and z axes, respectively. Crystal B was homogeneously modified through indiffusion using a different recipe but the same type of electrodes. This crystal resulted in a uniform appearance with dimensions of $5.5 \times 5.5 \times 5$ mm^3 along the x, y, and z axes, respectively. An iron-enriched melt was used to grow these two crystals, with the amount of Fe in the melt being

1000 ppm for crystal A and 2000 ppm for crystal B. The results obtained in this article with two crystals (in the regions where indiffusion occurred) are qualitatively and quantitatively similar.

Two nearly counterpropagating pump waves impinge upon the sample with thickness ℓ through the z faces that make an angle of about 10° in the air with this axis (Fig. 1). The intensity ratio of the pump waves $r=I_2(\ell)/I_1(0)$ could be changed in a range from 1 to 100. Both beams are polarized in the incident plane. In such a geometry the coupling strength $\gamma\ell$ for nearly counterpropagating waves is about 4.0–4.5.

The TEM_{00} radiation of multimode Ar^+-laser (λ =514 nm, output power ≈200 mW) is used as a pump source. The short coherence length of this laser easily allows for the two pump waves to be mutually incoherent. Both beams are tightly focused by lenses with a 1 m focal length (not shown in Fig. 1); the crystal is placed 1 cm before the focal point.

The spatial structure of generated light beams is observed on the screen SC placed at 32 cm behind the sample. A small circular aperture in the screen allows for passing pump wave 2 to the sample and fixes its direction, which is not changed in the experiment. Distinct from pump wave 2, the other pump wave 1 can be tilted. A mirror M mounted on the piezodriven holder allows for changing the angle θ of the reflected beam within a range approximately 100 mrad. The light spot on the mirror is imaged with the symmetric $F-F-F-F$ telescope into the sample, with the focal length F of the telescope lenses being 4 cm. This ensures the control of the pump intersection angle θ without affecting the overlap between the two pump waves (see [2]).

The direction opposite to wave 2 is taken as zero reference; the angle of the pump wave misalignment θ and angle of the oscillation wave propagation ϕ are measured from this reference direction. The oscillation waves that propagate in the direction close to direction of pump wave 2 are not shown so to avoid overloading Fig. 1. In the experiment one of them is used to measure the dynamics of oscillation intensity.

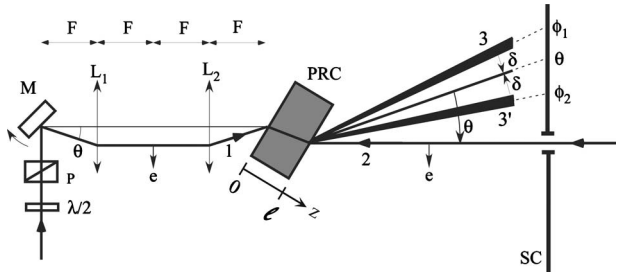

Fig. 1. Schematic representation of the experimental arrangement. Pump waves 1 and 2 enter the photorefractive crystal (PRC) from opposite faces. The lenses L_1 and L_2 with focal lengths F form a symmetric telescope that projects the image of a mirror M into the photorefractive sample PRC. The misalignment of the pump waves is adjusted by the tilt of the mirror M. Pump wave 2 enters the sample through a small aperture in the screen SC, which is used for monitoring the angular positions of pump wave 1 (θ) and oscillation waves 3 (ϕ_1) and 3′ (ϕ_2), with δ being the angle between pump wave 1 and oscillation waves 3 and 3′. All waves are polarized in the plane of the drawing, **e** being the polarization unit vector.

Most often the oscillation waves appear like speckled bright arcs that are normal to the plane of propagation for the pump waves. The brightest parts of the arcs are close to this plane. For pump misalignment in the horizontal plane the oscillation arcs are vertical [Fig. 2(a)], while for pump misalignment in the vertical plane they are horizontal. With a tilt of plane of the pump waves' intersec-

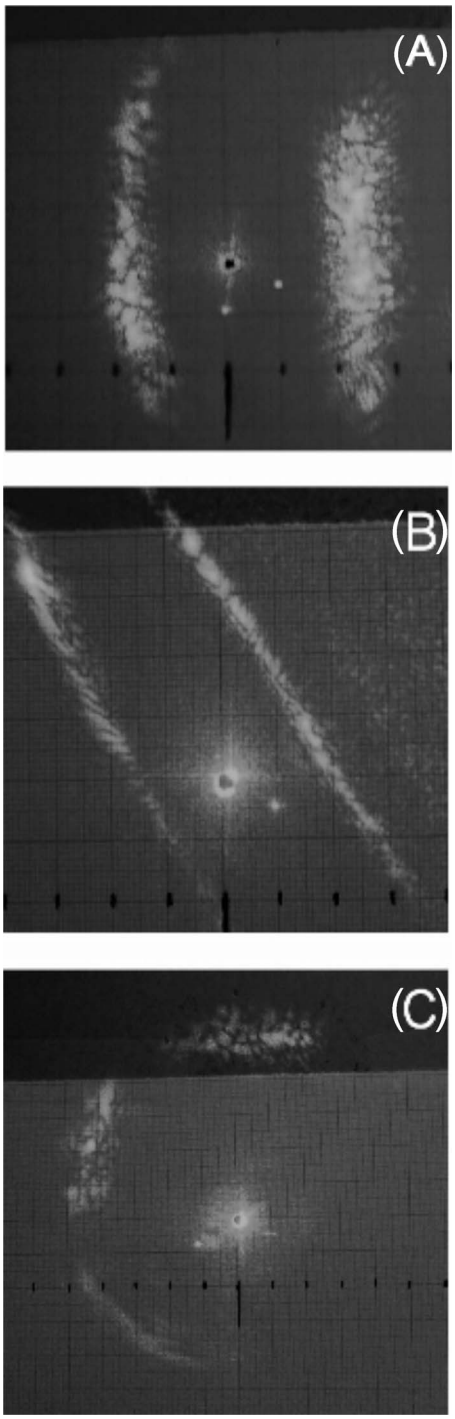

Fig. 2. Far-field oscillation patterns of crystal A. Two pump waves are (A) misaligned to 3 mrad in the horizontal plane, (B) misaligned to 5 mrad in a plane tilted to ≈30° with respect to the horizontal plane, and (C) aligned nearly perfectly. Pump ratio r =5. Total change of angle within frames A and B is 250 mrad, while within frame C it is 400 mrad.

tion the arcs are tilted too, but in the orthogonal direction [Fig. 2(b)].

The oscillation pattern changes qualitatively when the pump misalignment angle approaches zero $\theta \to 0$: the lines become curved and for perfect alignment they form a ring, i.e., the oscillation waves propagate along the conical surface with the axis defined by the pump wave direction. This cone is never filled with light homogeneously [Fig. 2(c)]; quite often only a fragment of conical radiation is seen.

All bright arcs are linearly polarized, identical to the polarization of the pump waves. The arcs get their intensity through the diffraction of the counterpropagating pump wave from the reflection grating. This is proved by checking the reaction of the arcs intensity to a sudden interruption of the pump wave. If a copropagating pump wave is stopped, the intensity of the scattered arcs decays gradually, following the decrease of the grating amplitude. In the case of a counterpropagating pump wave that is stopped, the arcs disappear instantaneously.

The intensity of the oscillation wave depends critically on the pump intensity ratio $r = I_2(\ell)/I_1(0)$. To change r the half-wave phase retarder $\lambda/2$ followed by the polarizer P are placed in the path of the pump wave 1. The rotation of the phase retarder allows for reducing the transmitted intensity, while keeping the polarization the same, parallel to the polarization of the pump wave 2. The phase retarder is mounted on a holder driven by a step motor, which ensures highly precise and slow variation of the pump intensity, practically with no mechanical vibrations. The rotation velocity is small, one full rotation cycle per hour, in order to ensure adiabatically slow variations of the pump ratio.

The raw results for crystal A are presented in Fig. 3(a) where the temporal variations of oscillation wave intensity $I_4(0)$ and pump wave intensity $I_1(0)$ are shown by curves 1 and 2, respectively. The intensity of the pump wave varies accordingly to $\cos^2 2\alpha$, where α is a phase-retarder rotation angle that increases linearly in time. When the intensity $I_1(0)$ smoothly approaches its minimum, the intensity $I_4(0)$ shows an abrupt drop. It is followed later by the abrupt switch-on, when the intensity $I_1(0)$ starts to increase, thus indicating the existence of the threshold value of the pump ratio over which the oscillation does not develop. Note also that the irregular spiking above the threshold disappears below the threshold.

Figure 3(b) represents the pump ratio dependence of the oscillation intensity reconstructed from data in Fig. 3(a). The oscillation intensity drops more than one order of magnitude over a range of r from 12 to 15. For larger r the signal-to-noise ratio becomes poor. The intensity decreases there roughly linearly with the decreasing $I_1(0)$, i.e., the detector is measuring the straight light of the scattered pump wave 1. A similar pump ratio dependence is observed with crystal B.

The other feature that supports the identification of the discovered emission as a coherent oscillation is a characteristic time delay in appearance of oscillation after starting of sample exposure to the pump light.

To measure the dependence of the oscillation wave direction on the pump misalignment angle θ a movie of the

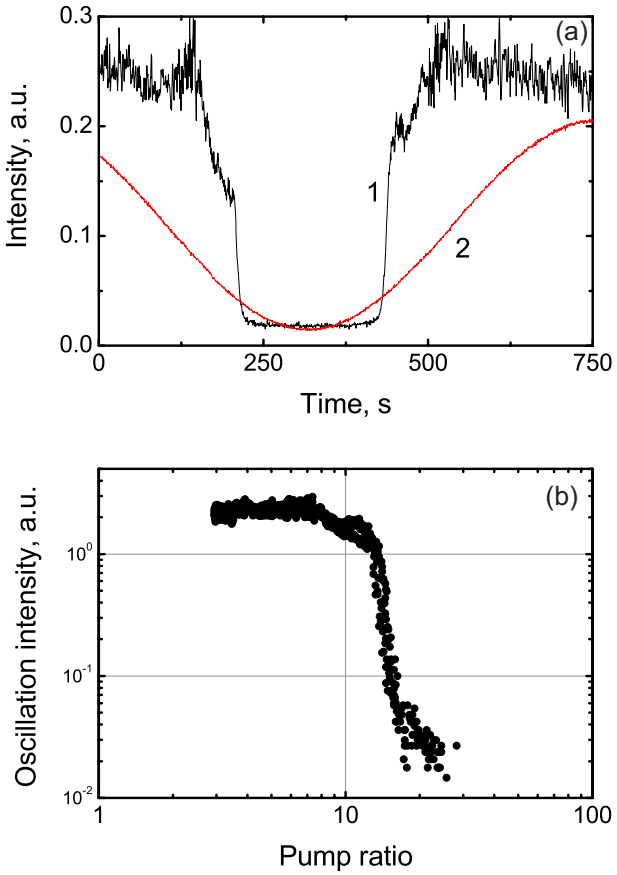

Fig. 3. (Color online) (a) Temporal variation of the mirrorless oscillation intensity (curve 1) in crystal A with slowly varying intensity of the pump 1 (curve 2). An abrupt disappearance and reappearance of the oscillation intensity prove the existence of the oscillation threshold in pump ratio. (b) Dependence of mirrorless oscillation intensity on the pump ratio, reconstructed from Fig. 3(a).

intensity distribution on the screen is recorded with a CCD camera. For large tilt angles of pump wave 1 the bright spot of the transmitted pump on the screen is well seen and corresponding angles can be calculated. This makes it possible to calibrate the angles for a whole movie, i.e., to attribute an exact value of θ to every movie frame. This is especially important for small values of θ, for which the bright spot falls into the aperture in the screen, through which the pump wave 2 passes, and becomes therefore invisible.

With such a technique the dependence shown in Fig. 4 is constructed for the oscillation of the crystal B. The vertical bars show the position and the angular width of the oscillation wave. It is clear that with an increasing θ the angular separation between two oscillation waves becomes smaller. They both approach the dashed straight line $\phi = \theta$ in Fig. 4. For a particular angle $\theta \simeq \pm 13$ mrad, one of two oscillation waves is exactly parallel to the counterpropagating pump wave. At this point the tilt angle ϕ of the oscillation wave passes zero value and changes its sign.

The dependence $\phi = \phi(\theta)$ measured for crystal A coincides with that shown in Fig. 4 within the experimental error bars. It shows a larger apex angle of conical oscillation $\delta_0 \approx 200$ mrad at $\theta = 0$.

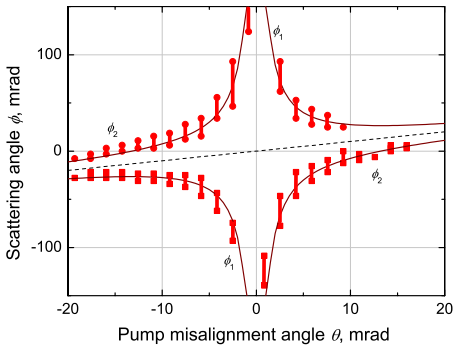

Fig. 4. (Color online) Dependence of the oscillation wave angle on pump misalignment angle for crystal B. The solid lines represent the best fit of the calculated dependence to the measured data shown by the vertical bars.

3. ANALYSIS OF THE PHASE-MATCHING CONDITION

The spatial structure of the observed patterns and their response to pump misalignment allows them to be attributed to $A:ee-ee$ parametric four-wave mixing according to classification given in [9]. Here the first two letters e mark the extraordinary polarization of the pump waves and the second pair of letters e mark the polarization of the scattered waves. One important distinction is, however, the necessity of the phase mismatch for optimizing the parametric gain. This distinction results in *a qualitatively new feature*: in lateral spatial split and lateral shift of the scattered light arcs with respect to the copropagating pump wave (Fig. 1).

The phase-matching condition for such a modified process A is as follows:

$$(\mathbf{k}_1 - \mathbf{k}_4) - (\mathbf{k}_3 - \mathbf{k}_2) = \mathbf{K}_1 - \mathbf{K}_2 = \mathbf{\Delta}, \tag{1}$$

where $\mathbf{k}_{1,2}$ are the wave vectors of the pump waves 1 and 2 and $\mathbf{k}_{3,4}$ are the wave vectors of the scattered waves 3 and 4. Two pump waves are mutually incoherent and the sample is aligned in a way to promote the recording of the reflection gratings. This is why the pump wave 1 records a grating with the grating vectors $\mathbf{K}_1$ together with the backscattered wave 4, while pump wave 2 together with wave 3 records another grating, with the grating vector $\mathbf{K}_2$. The two grating vectors are parallel to each other; their small difference defines the wave vector mismatch $\mathbf{\Delta}$.

Figure 5 shows two wave vector diagrams for opposite orientations of $\mathbf{\Delta}$ in the plane of propagation of the two pump waves. As one can see, for the same orientation of two pump waves 1 and 2, two orientations of the oscillation wave are possible, $3,3'$ (and $4,4'$ in the opposite direction); no preference exists and they both are observed in the experiment (see Fig. 2).

While the directions of the pump waves are imposed by the boundary conditions, the scattered waves may propagate in any direction that meets the above phase-matching condition, not only in the plane of the drawing in Fig. 5. This results in conical scattering with the cone axes close to the bisector of the two pump waves. On the screen behind the sample the scattering forms the arcs roughly normal to the plane of the pump wave intersection.

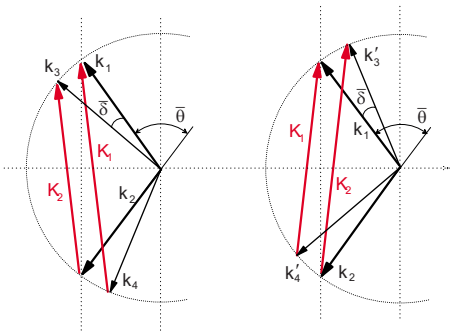

Fig. 5. (Color online) Ewald sphere constructions for phase-matching diagrams. All the wave vectors $\mathbf{k}_i$ have the same modulus $k=2\pi n/\lambda$. Grating vectors $\mathbf{K}_{1,2}$ are parallel and differ by $\mathbf{\Delta}$ in their length. Inside the sample the pump wave misalignment angle is $\bar{\theta}$ and the tilt angle of the oscillation wave with respect to the co-propagating pump wave is $\bar{\delta}$.

The tilt of the grating vectors $\mathbf{K}_{1,2}$ caused by pump misalignment is in fact very small, $\leq 10^{-2}$ rad. Within such a small angular window the two-beam coupling gain factor remains nearly the same regardless of the direction of the pump misalignment in the vertical or in the horizontal plane. This explains the observation of the horizontal arcs for vertical pump displacement and the tilted arcs for arbitrary plane of pump misalignment [Fig. 1(b)].

Wave vector diagrams of Fig. 5 and phase-matching condition, Eq. (1), allow for interrelating the angles $\phi_{1,2} = \theta \pm \delta$ of the oscillation waves' propagation and the pump misalignment angle θ with the relative wave vector mismatch Δ/k:

$$\phi_{1,2} \simeq \theta \pm \frac{n}{\theta}\left(\frac{\Delta}{k}\right), \tag{2}$$

where $k=2\pi/\lambda$ and n is the index of refraction.

This dependence describes qualitatively well the results of the experiment. A strong increase of the scattering angle ϕ with the pump misalignment angle that approaches zero is expected from Eq. (2), which is in agreement with the measured dependence shown in Fig. 4. Equation (2) predicts that one of the scattered waves should become parallel to the counterpropagating pump wave for a particular angle

$$\theta_{\|} = \delta = \sqrt{n\Delta/k}, \tag{3}$$

also in agreement with the experiment.

The fit of the experimental data in Fig. 4, according to Eq. (2), yields for normalized wave-vector mismatch a value $(n\lambda/2\pi)\Delta \approx 1.75\ 10^{-4}$. The estimated value of $\theta_{\|}$ from Eq. (3) is therefore $\approx$13 mrad. Also, the value of Δ extracted from this fit is $\Delta \approx 9.6\ \mathrm{cm}^{-1}$.

4. CALCULATIONS AND DISCUSSION

The equations that describe the temporal evolution of the backward wave four-wave mixing with phase mismatch and under the undepleted pump approximation have been considered in [6]

$$\frac{\partial A_3}{\partial z} = \nu^* \exp\left(-i\frac{\Delta z}{2}\right)A_2, \tag{4}$$

$$\frac{\partial A_4}{\partial z} = \nu \exp\left(-i\frac{\Delta z}{2}\right)A_1, \tag{5}$$

$$\tau\frac{\partial \nu}{\partial t} + \nu = \frac{\gamma^*}{I_0}\left[A_1^* A_4 \exp\left(i\frac{\Delta z}{2}\right) + A_2 A_3^* \exp\left(-i\frac{\Delta z}{2}\right)\right]. \tag{6}$$

Here z is the coordinate along the propagation axis, A_i are the complex amplitudes of the waves $i=1,2,3,4$, and A_i^* are their complex conjugates, γ is the coupling constant of the photorefractive crystal, ν is the grating amplitude, I_0 is the total intensity $I_0=|A_1|^2+|A_2|^2+|A_3|^2+|A_4|^2$, and τ is the response time of the photorefractive medium. The boundary conditions for the considered case are trivial. Only the nonzero amplitudes of the pump waves are fixed at the input faces.

The computer simulations of the sets of equations Eqs. (4)–(6) are performed, aiming to determine the areas of coupling strengths $\gamma\ell$ and dimensionless phase mismatches $\Delta\ell$ where the mirrorless oscillation can occur.

The numerical results allow for finding those sets of parameters $\gamma\ell$, r, and $\Delta\ell$ for which the intensity of wave 3 (and 4) takes a nonzero value in the steady state. They also allow for extracting the oscillation frequencies $\Omega_{1,2}$ from the beat frequency mark if the reference wave with the frequency of the pump wave is added.

In its present form the theory does not define the spatial orientation of the oscillation waves. One can assume, however, that the oscillation will occur in directions for which the difference $(\gamma\ell)$-$(\gamma\ell)_{th}$ of the coupling strength ensured by the crystal and the calculated threshold coupling strength is the largest possible. The seeding scattered light will be the most strongly amplified, and the oscillation will occur just in these directions. In distinction from the semilinear oscillator with two pump waves [10], here the phase condition of oscillation does not impose any additional constraints to the oscillation threshold because no feedback exists from the conventional cavity mirror.

Figure 6 shows the dependences of the threshold coupling strength $(\gamma\ell)_{th}$ and the dimensionless threshold frequency shift $\Omega\tau$ on phase mismatch $\Delta\ell$ for $r=5$. The pump ratio dependences of $\Delta\ell$ and Ω_{th} for $\gamma\ell=4.0$ are shown in Fig. 7.

It follows from the data in Fig. 6(a) that the smallest threshold coupling strength $\gamma\ell\approx3.7$ corresponds to the phase mismatch $\Delta\ell\approx4.5$, as it was stated already in [6]. The horizontal line in Fig. 6(a) marks the coupling strength $\gamma\ell=4$ for the crystal B (when it is tilted by an angle of $\approx10°$ relatively to two pump waves). The intersection points of this line and the coupling strength dependence define the range of phase mismatch in which the threshold condition of oscillation can be met. We believe, however, that the competition of different angular components for which the threshold is overcome will result in selection of the oscillation wave with smallest threshold value $\gamma\ell\approx3.7$ and direction of propagation defined by $\Delta\ell\approx4.5$. With crystal thickness $\ell=0.5$ cm the expected modulus of the wave-vector mismatch should be

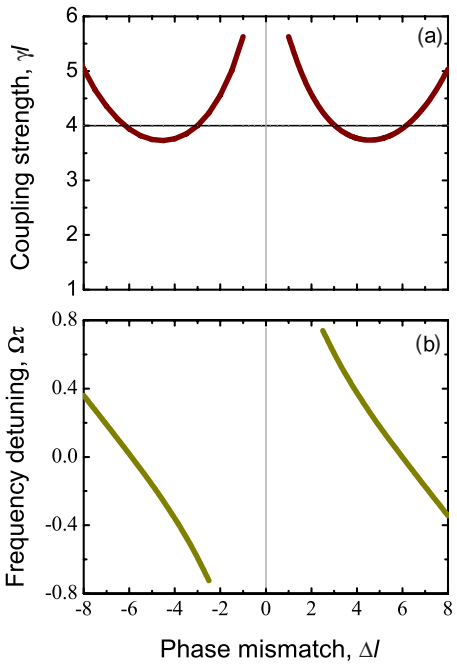

Fig. 6. (Color online) Calculated phase-mismatch dependences of (a) the threshold coupling strength and (b) the threshold frequency shift for mirorrless oscillation with the pump ratio close to optimum, $r=5$.

$\Delta\approx9$ cm^{-1}. This value differs less than 10% compared to the value extracted from the experimental dependence of Fig. 4, $\Delta\approx9.6$ cm^{-1}. For a theory that contains no free parameter such an agreement is quite satisfactory.

The contour plots of Fig. 7 show the pump ratio range $2.2<r<15$ within which the mirrorless oscillation is possible for a crystal with $\gamma\ell=4$. This prediction is in good agreement with the experimental data of Fig. 3.

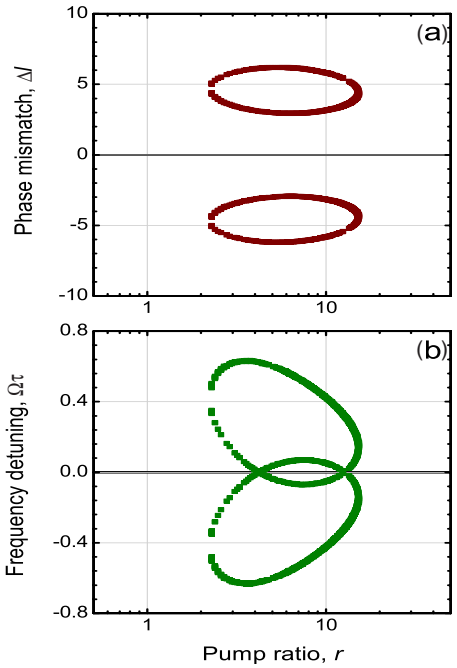

Fig. 7. (Color online) Calculated pump ratio dependences of (a) the threshold phase mismatch and (b) the threshold frequency shift for mirorrless oscillation with $\gamma\ell=4$.

While Eq. (2) describes well all experimental data of Fig. 4 with $\theta \neq 0$ it fails in explaining the ring structure observed with well-aligned pump waves. A conical scattering of counterpropagating pump waves with the cone axis along the pump propagation direction is usually attributed to parametric mixing of type B [9]. In this particular case it would be $B:ee-ee$ process with a modified phase-matching condition

$$(\mathbf{k}_1 - \mathbf{k}_2) - (\mathbf{k}_3 - \mathbf{k}_4) = \mathbf{\Delta}. \quad (7)$$

However, with $\mathbf{k}_1 \| \mathbf{k}_2$ the wave-vector mismatch $\mathbf{\Delta}$ is roughly perpendicular to the grating vectors $\mathbf{K}_1$ and $\mathbf{K}_2$ of partial gratings recorded by the pairs of coherent pump-and-scattering waves. Such a dephasing can hardly reduce the threshold for the coherent oscillation. The phase-matching condition of Eq. (7) can be met for $\theta = 0$ and $\mathbf{\Delta} = 0$, but in this case it does not impose any particular value to the apex angle of the scattered waves.

It is not excluded that the conical emission at $\theta = 0$ [Fig. 2(c)]is a consequence of finite and non-negligible divergence of counterpropagating pump waves that are focused into the sample with the converging lenses. With the beams' divergence of about 1 mrad one can expect a superposition of a multitude of bright arc pairs with angular spacing $\simeq 0.175$ rad within each pair (see Eq. (2) and the estimated value of Δ). Because of the axial symmetry, which is due to exact counterpropagation of two pump waves, the phase-matching condition of Eq. (1) does not impose any particular spatial orientation of the bright arc pairs. They fill, therefore, all possible azimuth angles in the viewing screen (in the far field), and their superposition results in an apparent ring. The apex angle of this ring, about 150 mrad, does not contradict this hypothesis.

5. CONCLUSIONS

The nonlinear scattering of two nearly counterpropagating mutually incoherent light waves into two pairs of bright arcs is attributed to be a consequence of the two simultaneous parametric four-wave processes of type $A:ee-ee$ (two extraordinary pump waves are mixed with two extraordinary scattered waves) with a slight positive/negative deviation from the exact phase matching.

The threshold dependence of the scattered intensity on the pump intensity ratio, the qualitative difference of temporal behavior (spiked below and smooth above the critical value of the pump intensity ratio), as well as the necessity to ensure quite large coupling strength to observe this effect, prove the manifestation of the absolute instability (mirrorless oscillation).

It is shown that the spatial orientation of the generated new beams is imposed by a modified wave-vector condition that admits possible spontaneous violation of the exact phase matching. The experimentally measured angular dependences are in good quantitative agreement with the prediction of a model.

ACKNOWLEDGMENT

S. Odoulov gratefully acknowledges the support of Université de Bourgogne during his stay as an invited professor in Dijon.

REFERENCES

1. R. Rebhi, P. Mathey, H. R. Jauslin, G. Cook, D. Evans, and S. Odoulov, "Four-wave-mixing coherent oscillator with frequency shifted feedback and misaligned pump waves," Opt. Lett. **34**, 377–379 (2009).
2. R. Rebhi, P. Mathey, H. R. Jauslin, G. Cook, D. Evans, D. Rytz, and S. Odoulov, "Dynamics of four-wave-mixing oscillators with quasi-phase-matching," Phys. Rev. A **7280**, 013803 (2009).
3. D. R. Evans, G. Cook, J. L. Carns, M. A. Saleh, S. A. Basun, J. M. Seim, and G. J. Mizell, "Major improvements in the photorefractive and photovoltaic properties in potassium niobate," Opt. Lett. **31**, 89–91 (2006).
4. C. Denz, J. Goltz, and T. Tschudi, "Enhanced four-wave mixing in photorefractive $BaTiO_3$ by use of tilted pump waves," Opt. Commun. **72**, 129–134 (1989).
5. N. V. Kukhtarev, T. I. Semenets, K. H. Ringhofer, and G. Tomberger, "Phase conjugation by reflection gratings in electrooptic crystals," Appl. Phys. B: Lasers Opt. **41**, 259–263 (1986).
6. R. Rebhi, P. Mathey, H. R. Jauslin, and B. Sturman, "Strong lowering of the mirrorless optical oscillation threshold by angular mismatches for nonlocal photorefractive nonlinearity," Opt. Lett. **33**, 2773–2775 (2008).
7. A. Yariv and D. Pepper, "Amplified reflection, phase conjugation, and oscillation in degenerate four-wave mixing," Opt. Lett. **1**, 16–18 (1977).
8. D. R. Evans, G. Cook, and M. A. Saleh, "Recent advances in photorefractive two-beam coupling," Opt. Mater. **31**, 1059–1060 (2009).
9. B. Sturman, S. G. Odoulov, and M. Y. Goul'kov, "Parametric four-wave processes in photorefractive crystals," Phys. Rep. **275**, 197–254 (1996).
10. P. Mathey, M. Grapinet, H. R. Jauslin, B. Sturman, D. Rytz, and S. Odoulov, "Threshold behavior of semi-linear photorefractive oscillator," Eur. Phys. J. D **39**, 445–451 (2006).